Energy spectra and oscillatory magnetization of two-electron self-assembled $In_xGa_{1-x}As$ quantum rings in GaAs

V. M. Fomin,* V. N. Gladilin,† and J. T. Devreese‡
Theoretische Fysica van de Vaste Stoffen, Departement Fysica, Universiteit Antwerpen, Groenenborgerlaan 171, B-2020 Antwerpen, Belgium

N. A. J. M. Kleemans and P. M. Koenraad
Photonics and Semiconductor Nanophysics, COBRA, Eindhoven University of Technology, P. O. Box 513, NL-5600 MB Eindhoven, The Netherlands

(Received 5 February 2008; revised manuscript received 23 April 2008; published 23 May 2008)

The effects of the Coulomb interaction on the energy spectrum and the magnetization of two electrons in a strained $In_xGa_{1-x}As/GaAs$ ringlike nanostructure are analyzed with realistic parameters inferred from the cross-sectional scanning-tunneling microscopy data. With an increasing magnetic field, the lowest spin-singlet and spin-triplet states sequentially replace each other as the ground state. This is reminiscent of the Aharonov–Bohm effect for the ringlike structures. The exchange interaction leads to a more complicated oscillatory structure of the magnetic moment of the two electrons as a function of the magnetic field as compared to the magnetization pattern for a single-electron ringlike nanostructure. We discuss the relevance of the two-electron systems for the interpretation of the Aharonov–Bohm oscillations in the persistent current observed in low temperature magnetization measurements on self-assembled $In_xGa_{1-x}As/GaAs$ ringlike nanostructures.

DOI: 10.1103/PhysRevB.77.205326 PACS number(s): 73.23.Ra, 71.15.−m, 73.21.La, 73.22.−f

I. INTRODUCTION

Electrons confined to a small ring manifest their quantum nature by an oscillatory behavior of their energy levels as a function of an applied magnetic field. This effect originates from the periodic dependence of the phase of the electron wave function on the magnetic flux through the ring, which is the Aharonov–Bohm effect,[1] and is usually associated with the occurrence of persistent currents in the ring.[2–5]

In recent years, the fabrication and the investigation of $In_xGa_{1-x}As$ self-assembled quantum rings (SAQRs) have been rapidly progressing, see, e.g., Refs. 6–10. The analysis of the shape, size, and composition of SAQRs at the atomic scale performed by cross-sectional scanning-tunneling microscopy (X-STM)[11,12] revealed that AFM only shows the material coming out of the quantum dots (QDs) during the quantum ring (QR) formation. The remaining parts of the QDs, as observed by X-STM, possess indium-rich craterlike shapes that are actually responsible for the ringlike properties of SAQRs. Recently, the magnetic moment has been measured at low temperature on a sample consisting of 29 layers of SAQRs, which are designed such that each quantum ring confines one or two electrons. By using an ultrasensitive torsion magnetometer in magnetic fields up to 15 T, the oscillatory persistent current in SAQRs has been observed.[13] It was explained using the theory of the electron energy spectra and the magnetization of a single-electron SAQR.[14]

The electron-electron interaction in the presence of disorder is known to be of key importance in the physics of persistent currents in quantum rings.[15–17] Because SAQRs are strongly anisotropic, the potential acting on electrons is analogous to that in an axially symmetric ring with imperfections (see e.g., Ref. 5). The purpose of the present paper is to study the contribution from SAQRs with two electrons to the magnetization.

To start with, we briefly recall the existing approaches to the analysis of persistent currents and related phenomena in quantum rings. On the one hand, the strong-correlation methods were actively developed within the framework of simple confinement models. The approach, which was developed for the ballistic regime,[18] was applied to a few-electron system, which is confined to a narrow-width quantum ring. The electrons form a strongly correlated system, which is a rotating nonrigid Wigner crystal. Within this approach, the energy band structure, the optical absorption, and the differential cross section of resonant Raman scattering of two interacting electrons were analyzed.[19] Evidence for a Wigner crystallization transition in the quantum rings, as the electron density is lowered, is found in a wide range of ring diameters and strengths of the harmonic confinement potential by using the Monte Carlo calculations.[20] The numerical solution for the electronic structure and the linear-response dynamics for the two-electron rings[21] is shown to correspond to a rotating Wigner molecule in narrow rings. A quantitative determination of the Wigner crystallization onset for the two electrons in a parabolic two-dimensional confinement has been provided.[22] The far-infrared transmission spectrum of InAs self-assembled nanoscopic rings obtained using the time-dependent local-spin-density theory[23] is in agreement with the experiment.[7]

On the other hand, numerical methods were extensively used, which allow for the investigation of advanced confinement models. In the early work,[24] the effect of the electron-electron interaction on the magnetic moment of electrons in a QR was studied by using a numerical solution for 4 to 12 electrons within the framework of a model with a parabolic confinement. The subsequent work implied that a parabolic confinement model is too restrictive for the realistic SAQRs.

Results of the exact diagonalization method[25] suggest a rich spectroscopic structure in the few-electron quantum

rings. The generalized Kohn theorem is not applicable for a ringlike confinement potential. The effects of electron-electron interaction of a two-electron nanoscopic ring on the energy levels and far-infrared spectroscopy have been investigated using an exact numerical diagonalization.[26] The solution of the Schrödinger equation for two electrons in a quantum ring with a circularly symmetric nonparabolic confinement potential was obtained in Ref. 27 by discretizing the coordinate space in a uniform grid of points. The height of the repulsive central barrier in the confining potential is shown to significantly influence the ring properties. The experiments[7] are explained invoking an additional assumption that both high- and low-barrier quantum rings are present in the sample.

Furthermore, the energy levels and far-infrared absorption spectra of a self-assembled InAs ring with one and two electrons in an external magnetic field are numerically calculated[28] using a three-dimensional effective mass model which considers finite potential barriers and mass dependence on the energy and position and includes strain effects. The obtained results suggest that the parabolic confinement potential used for mesoscopic rings is unsuitable for the self-assembled rings. However, the quantum-ring profile model[28] is azimuthally symmetric.

In the present paper, based on the structural information from the X-STM measurements, we calculate the electron energy spectra and the magnetization of a two-electron SAQR with a *realistic anisotropic singly connected shape* using a numerical diagonalization of the two-electron Hamiltonian within a finite basis of wave functions.

The paper is organized as follows. In Sec. II, a model of the SAQR is briefly presented, the physical problem is formulated, and a solution to the Schrödinger equation for a two-electron SAQR is presented. The effects of the Coulomb interaction on the electron energy spectra and the magnetization in a two-electron SAQR are discussed in Sec. III. Section IV contains the conclusions.

II. PROBLEM

A. Self-assembled quantum ring structure

An anisotropic craterlike SAQR structure is modeled with a varying-thickness $In_xGa_{1-x}As$ layer embedded in an infinite GaAs medium. The bottom of the $In_xGa_{1-x}As$ layer is considered to be perfectly flat and parallel to the xy plane. The height of the $In_xGa_{1-x}As$ layer as a function of the radial coordinate ρ and of the angular coordinate φ is modeled by the expression (1) of Ref. 14. The thickness at the center of the crater h_0 is nonzero, which means that the SAQR is a *singly connected* structure. The other relevant parameters of the model are h_M, the rim height, h_∞, the thickness of the $In_xGa_{1-x}As$ layer far away from the ringlike structure, γ_0 and γ_∞, the inner and outer slopes of the rim, respectively. The *anisotropy* of the rim height, the inner and outer slopes of the rim, and the characteristic radius is, correspondingly, described by Eqs. (2)–(5) of Ref. 14. The parameters ξ_h, ξ_γ, ξ_R determine the relative amplitudes of the azimuthal variations for the rim height, the slopes of the rim, and the characteristic radius of the structure.

The geometric parameters of the SAQR are $h_0=1.6$ nm, $h_\infty=0.4$ nm, $h_M=3.6$ nm, $\gamma_0=\gamma_\infty=3$ nm, and $R=10.75$ nm. The parameters, which describe the ring-shape anisotropy, are $\xi_h=0.2$, $\xi_\gamma=-0.25$, and $\xi_R=0.07$. An indium concentration of 55% results in a calculated surface relaxation that matches the experimentally determined relaxation of the cleaved surface.[12] This set of geometric and material parameters of the SAQR, which was selected for the analysis of the electron energy spectra in a single-electron SAQR,[14] is used here for the calculations of the electron energy spectra in the two-electron SAQR.

The Hamiltonian of the two electrons in the SAQR is represented as

$$H_{ee}(\mathbf{r}_1,\mathbf{r}_2) = H_1(\mathbf{r}_1) + H_2(\mathbf{r}_2) + V_{\mathrm{Coul}}(\mathbf{r}_1,\mathbf{r}_2), \tag{1}$$

where $H_1(\mathbf{r}_1)$ and $H_2(\mathbf{r}_2)$ correspond to the single-electron Hamiltonian (see Sec. II B) and $V_{\mathrm{Coul}}(\mathbf{r}_1,\mathbf{r}_2)$ describes the Coulomb interaction between the electrons with radius vectors $\mathbf{r}_1$ and $\mathbf{r}_2$.

B. Single-electron states in a self-assembled quantum ring

The solution of the single-electron problem in a SAQR has been provided in Ref. 14. Here, we recall the main conceptual ingredients of the solution of the single-electron problem in the SAQR, which are needed below for the treatment of the two-electron SAQR. Using the results of Refs. 29 and 30, we take the Hamiltonian of an electron in a strained ring in the form given by the expression (6) of Ref. 14. The components of the strain tensor, as well as the spatial distribution of indium x for the above described geometry of a SAQR, were obtained using a three-dimensional finite-element numerical calculation package ABAQUS,[31] which is based on elasticity theory. Using the calculated components of the strain tensor and x, we numerically calculate and tabulate the distributions of the strain-induced shifts of the conduction band edge and of the piezoelectric potential, which are given by the expressions (7) and (8) of Ref. 14, respectively. The electron band mass for $In_xGa_{1-x}As$ is taken from a linear interpolation between the corresponding values for InAs and GaAs.

The single-electron Schrödinger Eq. (9) of Ref. 14 is solved within the adiabatic approximation, using the Ansatz:

$$\Psi_{kj}^{(e)}(\mathbf{r}) = \psi_k^{(e)}(z;\rho,\varphi)\Phi_{kj}^{(e)}(\rho,\varphi), \tag{2}$$

where the index k numbers subbands due to the size quantization along the z axis and the index j labels the eigenstates of the in-plane motion. The Schrödinger equation for the "fast" degree of freedom (along the z axis) is numerically solved for each node of a two-dimensional grid in the (ρ,φ) plane. The resulting adiabatic potential, which corresponds to the lowest (with $k=1$) subband of the strong size quantization along the z axis, is plotted in Fig. 3 of Ref. 14. Due to strain, the depth of the adiabatic potential for an electron significantly decreases and its anisotropy diminishes.

For each value of the applied magnetic field, the eigenfunctions $\Phi_{1j}^{(e)}(\rho,\varphi)$ of the in-plane motion are found by numerical diagonalization of the adiabatic Hamiltonian for the "slow" degrees of freedom in the finite basis of the Fock–

Darwin wave functions. The wave functions of the lowest single-electron states in the SAQR result in the form

$$\Psi_{1j}^{(e)}(\mathbf{r}) = \psi_1^{(e)}(z;\rho,\varphi) \sum_{L=-L_{\max}}^{L_{\max}} \chi_{1jL}^{(e)}(\rho) e^{iL\varphi}. \tag{3}$$

Due to the anisotropic shape of the SAQR, angular momentum L is not a good quantum number and the basis set (3) represents a mixture of states with different values of L. The radial wave functions $\chi_{1jL}^{(e)}(\rho)$ are found in Ref. 14 for different angular momenta $L=-L_{\max},\ldots,L_{\max}$, where $L_{\max}=12$. The index $j=1,2,3,\ldots$ labels single-electron eigenstates in the order of increasing energy. In the case of vanishing anisotropy, the correspondence between the index j at $H=0$ and the angular momenta is as follows: $j=1\rightarrow L=0, j=2\rightarrow L=-1, j=3\rightarrow L=1, j=4\rightarrow L=-2, j=5\rightarrow L=2$, etc.

C. Two electrons

In order to obey the Pauli exclusion principle, the spin-singlet (spin-triplet) states in the two-electron rings must possess orbital wave functions which are symmetric (antisymmetric) with respect to the permutation of the coordinates of electrons. Aimed at finding two-electron eigenstates, we start, as a preparatory step, with constructing the basis functions, which describe the orbital wave functions of spin-singlet and spin-triplet states in the absence of the electron-electron interaction:

$$\Psi_{j_1j_2}^{(ee,0)}(\mathbf{r}_1,\mathbf{r}_2) = c_{j_1j_2}[\Psi_{1j_1}^{(e)}(\mathbf{r}_1)\Psi_{1j_2}^{(e)}(\mathbf{r}_2) + \Psi_{1j_1}^{(e)}(\mathbf{r}_2)\Psi_{1j_2}^{(e)}(\mathbf{r}_1)], \tag{4}$$

$$\Psi_{j_1j_2}^{(ee,1)}(\mathbf{r}_1,\mathbf{r}_2) = c_{j_1j_2}[\Psi_{1j_1}^{(e)}(\mathbf{r}_1)\Psi_{1j_2}^{(e)}(\mathbf{r}_2) - \Psi_{1j_1}^{(e)}(\mathbf{r}_2)\Psi_{1j_2}^{(e)}(\mathbf{r}_1)], \quad j_1 \neq j_2, \tag{5}$$

where $c_{j_1j_2}=1/\sqrt{2}$ for $j_1\neq j_2$ and $c_{j_1j_1}=1/2$. In the present calculations, this basis corresponds to $j_1,j_2=1,\ldots,j_{\max}$, where $j_{\max}=9$ and contains $j_{\max}(j_{\max}+1)/2=45$ functions for spin-singlet states and $j_{\max}(j_{\max}-1)/2=36$ functions for spin-triplet states. We diagonalize the Hamiltonian (1) in the above basis looking for the wave functions of the two interacting electrons in the form

$$\tilde{\Psi}_J^{(ee,S)}(\mathbf{r}_1,\mathbf{r}_2) = \sum_{j_1=1}^{j_{\max}} \sum_{j_2=1}^{j_1-S} A_{Jj_1j_2} \Psi_{j_1j_2}^{(ee,S)}(\mathbf{r}_1,\mathbf{r}_2), \tag{6}$$

where $S=0$ ($S=1$) in the case of spin-singlet (spin-triplet) states.

When calculating matrix elements of the Coulomb interaction $V_{\text{Coul}}(\mathbf{r}_1,\mathbf{r}_1)$ in the basis (4) and (5), it is convenient to represent them as

$$(V_{\text{Coul}})_{j_1,j_2,i_1,i_2}^{(S)} = \int d^3\mathbf{r}_e \int d^3\mathbf{r}_h [\Psi_{j_1j_2}^{(ee,S)}(\mathbf{r}_1,\mathbf{r}_2)]^* \times V_{\text{Coul}}(\mathbf{r}_1,\mathbf{r}_2)\Psi_{i_1i_2}^{(ee,S)}(\mathbf{r}_1,\mathbf{r}_2)$$
$$= 2c_{j_1j_2}^2 c_{i_1i_2}^2 \sum_{L_{j1},L_{j2},L_{i1},L_{i2}=-L_{\max}}^{L_{\max}} \int_0^\infty d\rho_1 \int_0^\infty d\rho_2$$
$$\times [\chi_{1j_1L_{j1}}^{(e)}(\rho_1)\chi_{1j_2L_{j2}}^{(e)}(\rho_2)]^*$$
$$\times \{\chi_{1i_1L_{i1}}^{(e)}(\rho_1)\chi_{1i_2L_{i2}}^{(e)}(\rho_2)\tilde{S}_{L_{i1}-L_{j1},L_{i2}-L_{j2}}(\rho_1,\rho_2)$$
$$\pm \chi_{1i_1L_{i1}}^{(e)}(\rho_2)\chi_{1i_2L_{i2}}^{(e)}(\rho_1)\tilde{S}_{L_{i2}-L_{j1},L_{i1}-L_{j2}}(\rho_1,\rho_2)\}, \tag{7}$$

where the upper (lower) sign in the rhs corresponds to $S=0$ ($S=1$) and

$$\tilde{S}_{\Delta L_1,\Delta L_2}(\rho_1,\rho_2) = \frac{e^2\rho_1\rho_2}{4\pi\varepsilon_0\varepsilon_r} \int_0^{2\pi} d\varphi_1 \int_0^{2\pi} d\varphi_2 \int_{-\infty}^{\infty} dz_1 \int_{-\infty}^{\infty} dz_2 \times |\psi_1^{(e)}(z_1;\rho_1,\varphi_1)|^2 |\psi_1^{(e)}(z_2;\rho_2,\varphi_2)|^2 \times \frac{e^{i\Delta L_1\varphi_1 + i\Delta L_2\varphi_2}}{\sqrt{\rho_1^2+\rho_2^2-2\rho_1\rho_2\cos(\varphi_1-\varphi_2)+(z_1-z_2)^2}}. \tag{8}$$

Importantly, the integrals $\tilde{S}_{\Delta L_1,\Delta L_2}(\rho_1,\rho_2)$ do not depend on the magnetic field. Therefore, we first tabulate $\tilde{S}_{\Delta L_1,\Delta L_2}(\rho_1,\rho_2)$. Then, for each magnetic field H, the matrix elements (7) are calculated and the lowest two-electron states are found by numerical diagonalization of the Hamiltonian (1) in the basis (4) and (5).

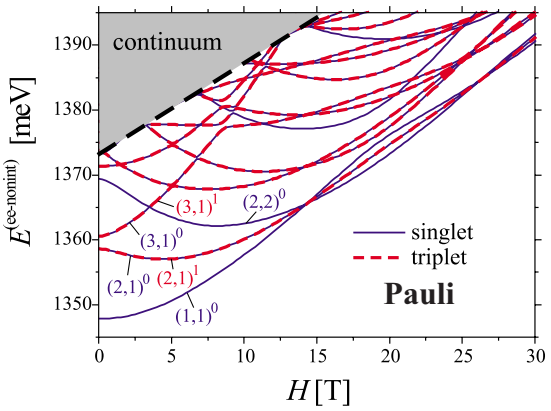

FIG. 1. (Color online) Energy spectrum of two noninteracting electrons in a strained quantum ring as a function of the applied magnetic field. The states $\Psi_{j_1j_2}^{(ee,S)}$ for $S=0,1$ are labeled as $(j_1,j_2)^S$, where the numbers j_1 and j_2 correspond to the order of the single-electron energy levels at $H=0$. All triplet energy levels $(j_1,j_2)^1$ for $j_1\neq j_2$ overlap with singlet energy levels $(j_1,j_2)^0$. The heavy dashed line, which indicates the region of the continuum as obtained from our numerical simulation, is a guide to the eye.

III. RESULTS

The states $\Psi_{j_1j_2}^{(ee,S)}$ for $S=0,1$ are labeled as $(j_1,j_2)^S$, where the numbers j_1 and j_2 correspond to the order of the single-electron energy levels at $H=0$. The states $\tilde{\Psi}_J^{(ee,S)}$ are labeled as $(J)^S$ for $S=0,1$.

In Figs. 1 and 2, the calculated two-electron energy spectra are plotted for the cases, respectively, of no electron-electron interaction and with the Coulomb interaction taken

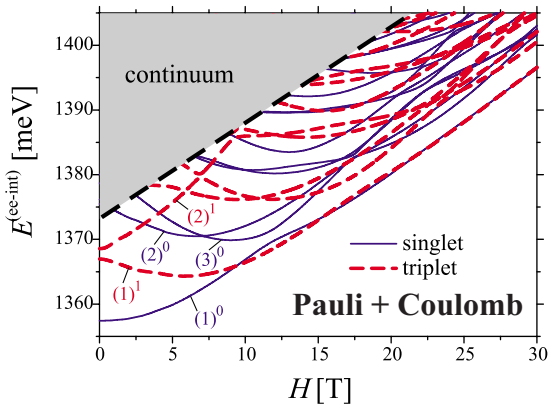

FIG. 2. (Color online) Energy spectrum of two electrons in a strained quantum ring as a function of the applied magnetic field in the case when the Coulomb interaction is taken into account. The states $\tilde{\Psi}_J^{(ee,S)}$ are labeled as $(J)^S$ for $S=0,1$. The heavy dashed line, which indicates the region of the continuum as obtained from our numerical simulation, is a guide to the eye.

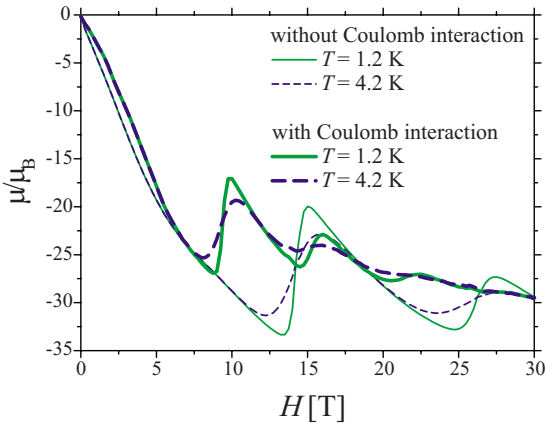

FIG. 3. (Color online) The calculated magnetic moment of two noninteracting (interacting) electrons in a strained quantum ring is shown by the thin (heavy) lines for two different temperatures.

into account. The Pauli exclusion principle is fulfilled when constructing the wave functions (4)–(6), which are used to calculate the energy levels shown in Figs. 1 and 2.

In Fig. 1, the spin-singlet $(j_1,j_2)^0$ and spin-triplet states $(j_1,j_2)^1$ are degenerate because the Coulomb interaction is not taken into account. It is worth recalling here that the index j, rather than the electron angular momentum L, is specific for single-electron eigenstates in an anisotropic quantum ring. Due to the Coulomb interaction, the energy spectrum of two electrons represented in Fig. 2 is significantly modified as compared to that shown in Fig. 1. Approximately, the correspondence between the states of two electrons in a quantum ring with the Coulomb interaction and the states of two noninteracting electrons in a quantum ring is as follows: $(1,1)^0 \rightarrow (1)^0$; $(2,1)^0 \rightarrow (2)^0$; $(2,2)^0 \rightarrow (3)^0$; $(2,1)^1 \rightarrow (1)^1$; $(3,1)^1 \rightarrow (2)^1$.

As follows from Fig. 2, the degeneracy between the spin-singlet and spin-triplet states is lifted due to the Coulomb interaction. For example, there is a significant splitting between the spin-singlet $(2)^0$ and the spin-triplet $(1)^1$ states, although the corresponding states of two noninteracting electrons $(2,1)^0$ and $(2,1)^1$ are degenerate. This fact indicates a strong exchange interaction in the quantum ring under consideration.

At relatively low magnetic fields, the ground state in Fig. 2 corresponds to the lowest spin-singlet energy level. At $H \approx 10$ T, the ground state becomes spin triplet. With a further increase in magnetic field, the lowest spin-singlet and spin-triplet states sequentially replace each other as the ground state. This behavior is reminiscent of the Aharonov–Bohm effect in a single-electron quantum ring. At $H \approx 12$ T, the state originating from $(1,1)^0$ reveals anticrossing from those states which originate from $(2,1)^0$ and $(2,2)^0$. Different energy levels corresponding to the abovementioned states are shifted differently due to the Coulomb interaction.

In Fig. 3, the calculated magnetic moment μ of the two noninteracting and interacting electrons is plotted as a function of the applied magnetic field. As seen from Fig. 3, the Coulomb interaction leads to a more complicated oscillating structure of μ versus H, as compared to the case when the electron-electron interaction is absent. In particular, the first oscillation of the magnetic moment shifts due to the Coulomb interaction toward the weaker magnetic fields. One of the reasons for this shift is an increase in the effective electronic radius of the ring due to the mutual Coulomb repulsion of the two electrons. At $H > 15$ T, the Aharonov–Bohm oscillations of the magnetic moment are still present but are substantially smoothed out.

IV. CONCLUSION

In conclusion, the major effect of the Coulomb interaction is lifting the degeneracy between the spin-singlet and spin-triplet states. For the two-electron quantum rings with radial sizes ~ 10 nm, the Aharonov–Bohm-effect-related phenomena appear at magnetic fields ~ 10 T even in the case of an appreciable shape anisotropy. In the experiment on magnetization in SAQRs with those sizes and shape,[13] no appreciable oscillations are detected in the above region. Therefore, it is assumed that the observed Aharonov–Bohm effect is mainly due to the single-electron quantum rings in the ensemble of rings under investigation.

ACKNOWLEDGMENTS

The authors thank P. Offermans for performing some of the numerical calculations of the strain field. They acknowledge their collaboration with J. M. García, D. Granados, A. G. Taboada, J. H. Blokland, I. M. A. Bominaar-Silkens, P. C. M. Christianen, J. C. Maan, and U. Zeitler. This work was supported by the FWO-V Projects No. G.0115.06 and No. G.0356.06, the WOG Grant No. WO.035.04N (Belgium), the nanotechnology program of the Dutch Ministry of Economic Affairs NanoNed (The Netherlands), and the EC Network of Excellence SANDiE Contract No. NMP4-CT-2004-500101.

*Also at Photonics and Semiconductor Nanophysics, COBRA, Eindhoven University of Technology, P.O. Box 513, 5600 MB Eindhoven, The Netherlands. On leave from Physics of Multilayer Structures, Department of Theoretical Physics, State University of Moldova, A. Mateevici 60, MD-2009 Chişinău, Moldova.

†Also at Vaste-Stoffysica en Magnetisme, Katholieke Universiteit Leuven, Celestijnenlaan 200 D, B-3001 Leuven, Belgium. On leave from Physics of Multilayer Structures, Department of Theoretical Physics, State University of Moldova, A. Mateevici 60, MD-2009 Chişinău, Moldova.

‡Also at Photonics and Semiconductor Nanophysics, COBRA, Eindhoven University of Technology, P.O. Box 513, 5600 MB Eindhoven, The Netherlands.

[1] Y. Aharonov and D. Bohm, Phys. Rev. **115**, 485 (1959).

[2] N. Byers and C. N. Yang, Phys. Rev. Lett. **7**, 46 (1961).

[3] F. Bloch, Phys. Rev. B **2**, 109 (1970).

[4] M. Büttiker, Y. Imry, and R. Landauer, Phys. Lett. **96**, 365 (1983).

[5] L. Wendler, V. M. Fomin, and A. A. Krokhin, Phys. Rev. B **50**, 4642 (1994).

[6] J. M. García, G. Medeiros-Ribeiro, K. Schmidt, T. Ngo, J. L. Feng, A. Lorke, J. Kotthaus, and P. M. Petroff, Appl. Phys. Lett. **71**, 2014 (1997).

[7] A. Lorke, R. J. Luyken, A. O. Govorov, J. P. Kotthaus, J. M. Garcia, and P. M. Petroff, Phys. Rev. Lett. **84**, 2223 (2000).

[8] R. J. Warburton, C. Schäflein, D. Haft, F. Bickel, A. Lorke, K. Karrai, J. M. García, W. Schoenfeld, and P. M. Petroff, Nature (London) **405**, 926 (2000).

[9] R. J. Warburton, C. Schulhauser, D. Haft, C. Schäflein, K. Karrai, J. M. García, W. Schoenfeld, and P. M. Petroff, Phys. Rev. B **65**, 113303 (2002).

[10] J. A. Barker, R. J. Warburton, and E. P. O'Reilly, Phys. Rev. B **69**, 035327 (2004).

[11] P. Offermans, P. M. Koenraad, J. H. Wolter, D. Granados, J. M. García, V. M. Fomin, V. N. Gladilin, and J. T. Devreese, Appl. Phys. Lett. **87**, 131902 (2005).

[12] P. Offermans, P. M. Koenraad, J. H. Wolter, D. Granados, J. M. García, V. M. Fomin, V. N. Gladilin, and J. T. Devreese, Physica E (Amsterdam) **32**, 41 (2006).

[13] N. A. J. M. Kleemans, I. M. A. Bominaar-Silkens, V. M. Fomin, V. N. Gladilin, D. Granados, A. G. Taboada, J. M. García, P. Offermans, U. Zeitler, P. C. M. Christianen, J. C. Maan, J. T. Devreese, and P. M. Koenraad, Phys. Rev. Lett. **99**, 146808 (2007).

[14] V. M. Fomin, V. N. Gladilin, S. N. Klimin, J. T. Devreese, N. A. J. M. Kleemans, and P. M. Koenraad, Phys. Rev. B **76**, 235320 (2007).

[15] V. Ambegaokar and U. Eckern, Phys. Rev. Lett. **65**, 381 (1990).

[16] N. Yu and M. Fowler, Phys. Rev. B **45**, 11795 (1992).

[17] N. Argaman and Y. Imry, Phys. Scr., T **49A**, 333 (1993).

[18] L. Wendler, V. M. Fomin, and A. V. Chaplik, Superlattices Microstruct. **16**, 311 (1994).

[19] L. Wendler, V. M. Fomin, A. V. Chaplik, and A. O. Govorov, Phys. Rev. B **54**, 4794 (1996).

[20] F. Pederiva, A. Emperador, and E. Lipparini, Phys. Rev. B **66**, 165314 (2002).

[21] A. Puente and L. Serra, Int. J. Quantum Chem. **86**, 27 (2002).

[22] H.-C. Wu, Y. Guo, X.-Y. Chen, and B.-L. Gu, Phys. Rev. B **68**, 125330 (2003).

[23] A. Emperador, M. Pi, M. Barranco, and A. Lorke, Phys. Rev. B **62**, 4573 (2000).

[24] T. Chakraborty and P. Pietiläinen, Phys. Rev. B **50**, 8460 (1994).

[25] V. Halonen, P. Pietiläinen, and T. Chakraborty, Europhys. Lett. **33**, 377 (1996).

[26] H. Hu, J.-L. Zhu, and J.-J. Xiong, Phys. Rev. B **62**, 16777 (2000).

[27] A. Puente and L. Serra, Phys. Rev. B **63**, 125334 (2001).

[28] J. I. Climente, J. Planelles, and F. Rajadell, J. Phys.: Condens. Matter **17**, 1573 (2005).

[29] J. A. Barker and E. P. O'Reilly, Phys. Rev. B **61**, 13840 (2000).

[30] M. Grundmann, O. Stier, and D. Bimberg, Phys. Rev. B **52**, 11969 (1995).

[31] http://www.simulia.com/products/abaqus_fea.html